Dynamically confined single-atom catalytic sites within a porous heterobilayer for CO oxidation via electronic antenna effects

Bojie Jiang,[1] Feixiang Zhang,[1] Yueyang Wang,[1] Xinlian Xue,[1] Jinlei Shi,[1] Xingju Zhao,[1] Lili Zhang,[1] Rui Pang,[1] Xiaoyan Ren,[1,*] Shunfang Li,[1,†] and Zhenyu Zhang[2,‡]

[1]*Key Laboratory of Material Physics, Ministry of Education, School of Physics and Microelectronics, Zhengzhou University, Zhengzhou 450001, China*

[2]*International Center for Quantum Design of Functional Materials (ICQD), Hefei National Laboratory for Physical Sciences at the Microscale, University of Science and Technology of China, Hefei, Anhui 230026, China*

(Received 9 June 2022; accepted 17 May 2023; published 30 May 2023)

Suppression of clustering of single-atom catalysts during chemical reaction is a long-standing challenge in heterogeneous catalysis, largely due to the prevailing design scheme that the catalytic atoms are anchored onto the supporting surfaces. Here we use first-principles approaches to establish a different design principle, where the single-atom catalytic centers are dynamically sandwiched between a porous g-C_3N_4/MoS_2 heterobilayer as a prototypical system. We show that many of the transition metals can be well stabilized as dispersive single atoms within the porous centers. Moreover, the single atoms migrate out of their sandwiched homes in O_2 activation and CO oxidation, and successfully return home after the reaction is completed. In such a dynamical process the single atoms function as electronic antennas, facilitating the charge donation to or acceptance from the reactants, while effectively lowering the reaction barriers. These findings are instructive in establishing high-performance single-atom catalysts upon two-dimensional porous materials.

DOI: 10.1103/PhysRevB.107.205421

I. INTRODUCTION

In recent decades, two important enabling concepts, i.e., single atom catalysis (SAC) [1–12] and confined catalysis [13–22], have been intensively exploited in the broad field of chemical catalysis. SAC, referring to the enhanced catalysis by single-atom catalysts with atomically deposited catalytic monomers stabilized on proper substrates, has surged to the forefront of heterogeneous catalysis due to the maximal atom utilization and abundant active sites [23–27]. In contrast to traditional nanocluster catalysts with different types of active sites [28–32] that otherwise may also promote undesirable side reactions, the systems in SAC could possess dramatically enhanced reaction selectivity owing to their specific coordination numbers and electronic structures [33–35]. As a pioneering example, Pt_1/FeO_x has been synthesized as a SAC system, with the single Pt atoms stabilized on the oxygen vacancy sites of FeO_x and exhibiting high stability and activity in CO oxidation [1]. Subsequently, various approaches have been applied to fabricate SAC systems, with the single-atom catalytic centers stabilized on defective surfaces [36,37], step edges [38,39], and alloys [40,41], which are essentially based on the concept of strong metal-support interactions established in 1978 [42] and developed as electronic metal-support interactions [43] coined by Campbell [44]. Such single-atomic catalytic systems were usually demonstrated to exhibit excellent catalysis for hydrogen evolution reaction [37,45,46], N_2 reduction [47,48], CO_2 reduction [49–51], or CO oxidation [1,5,9]. Yet to date, suppressing the aggregation of the single atoms during chemical reaction is a universal standing challenge [25,52], largely due to the prevailing design scheme that the catalytic atoms are anchored onto the surfaces of the supporting substrates.

Note that, confined catalysis has also been advocated as a complementary concept, referring to the enhanced catalysis enabled by the confined microenvironments of the heterogeneous catalysts within heterobilayers [13–22]. Essentially, the concept of confined catalysis is originated from the electronic quantum confinement effect in low dimensional nanostructures, which has endowed enormous exotic phenomena and applications in modern condensed matter physics, chemistry, and material science. For confined catalysis, the catalytic transitional metal structures are usually confined inside or underneath one- or two-dimensional protective materials such as nanotubes [18,53] or graphene [16,19,54], and exhibit inimitable advantages toward a variety of catalytic reactions, especially under harsh conditions, such as strong acidic or alkaline medium, high overpotential, and high temperature [17,54,55]. Crucially, when the sizes of the confined catalytic nanostructures are reduced to the single atom regime, the two concepts of SAC and confined catalysis converge, potentially allowing coherent integration of their merits for maximal catalytic performance [55–59]. However, in many cases, a dynamically flexible geometric structure and electronic configuration of a given catalytic site may be more desirable for high performance catalytic reactions [60,61].

Here we use first-principles approaches to establish a conceptually new design principle of SAC, termed dynamically

*Corresponding author: renxyan@zzu.edu.cn
†Corresponding author: sflizzu@zzu.edu.cn
‡Corresponding author: zhangzy@ustc.edu.cn

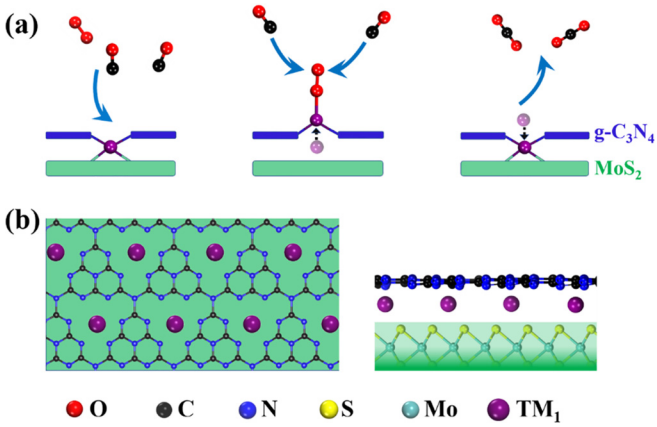

FIG. 1. Schematics of CO oxidation pathways on single-atom catalysts confined within a g-C_3N_4/MoS_2 heterobilayer. (a) Proposed CO oxidation processes on the TM_1@g-C_3N_4/MoS_2 heterobilayer wherein the transition metal single atom TM_1 is dynamically confined. (b) Top and side views of the single atoms confined in the interface of g-C_3N_4/MoS_2, with the MoS_2 represented by the green background.

confined SAC (DCSAC), by coherently integrating SAC and confined catalysis into a single heterogeneous catalytic platform. The principle is demonstrated using CO oxidation on single atoms sandwiched between a porous two-dimensional heterobilayer as a prototypical example. We first show that many transition metal atoms can be energetically well confined within the interface of an archetype heterobilayer of porous g-C_3N_4/MoS_2 which has already been experimentally fabricated [62]. Due to the confinement effect, the transition metal atoms prefer to be atomically dispersed rather than clustered, forming stable single-atom catalytic centers, upon which oxygen molecule adsorption and activation are found to preferentially proceed followed by efficient CO oxidation. Intriguingly, as schematically illustrated in Fig. 1(a), the single-atom catalytic centers adjust their vertical locations and coordination numbers dynamically during the reaction cycle, and returning to their stable interfacial homes after the reaction process is completed. Also importantly, the single atoms flexibly adapt their charge states in such a dynamic process, functioning as electronic "antennas" in the charge transfer process, which effectively lowers the energy barriers involved in CO oxidation. These findings are transformative in both condensed matter physics and environmental chemistry and beyond, with broad applications such as in integration and reutilization of toxic and noble elements.

The paper is organized as follows. The method and simulation details are presented in Sec. II. The results of our state-of-the-art simulations and discussion of the unique behaviors of the DCSAC serving as electronic antenna for CO oxidation are presented in Sec. III. We finally draw our conclusions and perspectives in Sec IV.

II. METHODS

Our calculations were carried out by spin-polarized first-principles calculations [63] based on density functional theory (DFT) as implemented in the Vienna *ab initio* simulation package (VASP) [64], with a projector augmented wave [65] method and Perdew-Burke-Ernzerhof (PBE) [66] for the exchange-correlation functional. Moreover, revised PBE functionals (RPBE) [67] was also compared and found to produce the same central findings. In our calculations, the g-C_3N_4/MoS_2 heterojunction was simulated by covering a 3×3 single-layer g-C_3N_4 on a 7×7 single-layer MoS_2. For such a large supercell in simulation of the semiconducting heterojunction, we adopted a $1 \times 1 \times 1$ Monkhorst Pack k-point mesh and an energy cutoff of 500 eV, which was found to lead good convergence within 0.02 meV/per atom. A vacuum layer of 15 Å in the z direction was used to ensure the decoupling between the neighboring images. The atomic positions were optimized by a conjugate gradient algorithm until the forces in all directions were less than 0.01 eV/Å and the convergence criterion for electronic step is within 10^{-4} eV. The optimized lattice constant of g-C_3N_4 is a $=$ b $= 6.96$ Å, in good agreement with previous experimental value [68]. The zero damping DFT-D3 method is adopted in describing van der Waals interactions [69,70]. Bader charge analysis is adopted to analyze charge transfer. To investigate the kinetic processes of the atom diffusion and CO oxidation, the climbing image nudged elastic band [71,72] method was used to identify the transition states and minimum energy paths. The thermodynamic stability of some typical TM_1@g-C_3N_4/MoS_2 complexes were also examined by *ab initio* molecular dynamic simulations performed at 500 K within a canonical ensemble using the algorithm of Nose.

III. RESULTS AND DISCUSSION

As a starting point, we briefly introduce the optimized geometric structure of the g-C_3N_4/MoS_2 heterobilayer as illustrated in Fig. 1(b) and detailed (see Sec. I of the Supplemental Material [73]). The optimized lattice constants of the buckled (flat) hexagonal g-C_3N_4 and MoS_2 monolayers are 6.960 (7.130) and 3.167 Å, respectively [68,74]. It is found that the buckled g-C_3N_4 is about 0.5 eV more stable than its flat counterpart per unit cell, however, when it is deposited on the MoS_2 in formation of a g-C_3N_4/MoS_2 heterobilayer, the g-C_3N_4 overlayer prefers to stay flat. In our simulations, considering the relatively flexible structure of the g-C_3N_4, we construct the g-C_3N_4/MoS_2 heterobilayer by placing hexagonal 3×3-g-C_3N_4 onto 7×7-MoS_2 with the optimized lattice constant of MoS_2, to minimize the lattice mismatch to about 3.6%. As shown in Fig. S1, five high-symmetry adsorption sites, i.e., the large hollow (H_1), small hollow (H_2), C top (T_C), N top (T_N), and bridge (B) between C and N are considered for the TM atom deposition onto the heterobilayer (see Sec. I of the Supplemental Material [73]).

To examine whether TM atoms prefer single-atomic dispersion or clustering in the heterobilayer, we have performed effective tests on the optimized configurations of three TM atoms introduced in the supercell. To also demonstrate the general validity of the present work, almost all the 3d-, 4d-, and 5d-TMs have been screened. As illustrated (see Sec. II of the Supplemental Material, Figs. S2 and S3 [73]), depending on the precise species of the TMs, five typical optimized configurations can be obtained for the three atoms, with the formations of (i) sevenfold-coordinated isolated single atoms

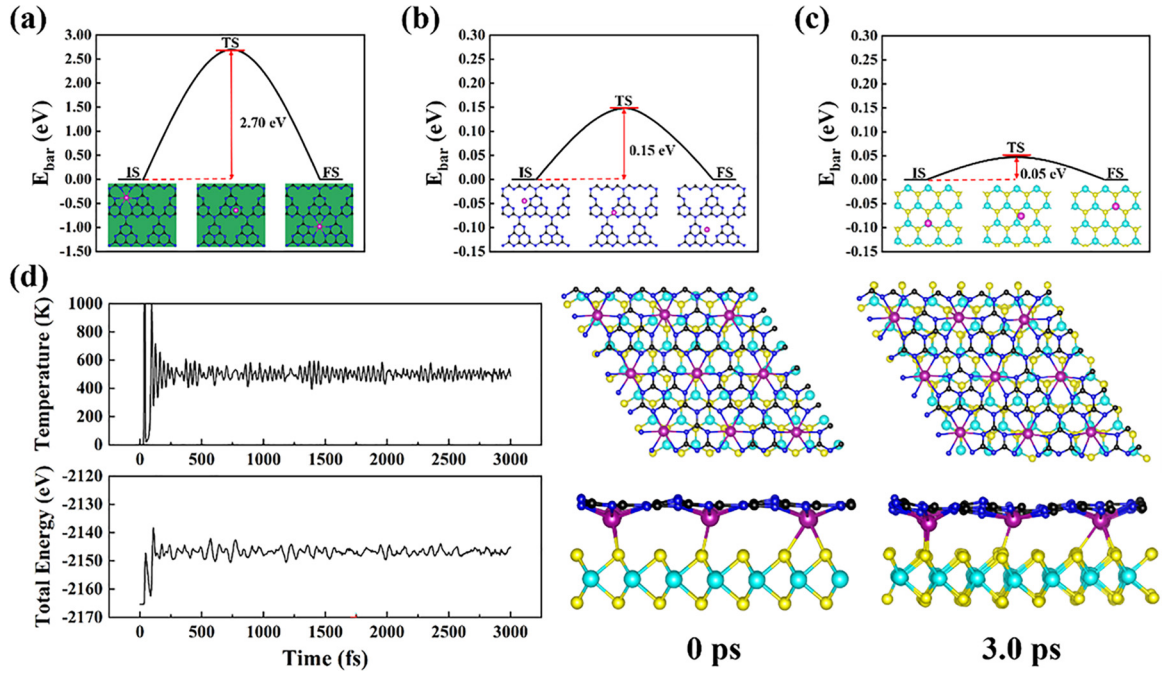

FIG. 2. Cd single atom diffusion when (a) it is confined in g-C_3N_4/MoS_2 heterobilayer; (b) on the surface of pristine MoS_2; (c) on the surface of pristine 2D g-C_3N_4. (d) Thermodynamic stability of the Cd_1@g-C_3N_4/MoS_2 complex examined by *ab initio* molecule dynamic simulations performed at 500 K. The representative snapshots of the geometric structures in both top and side views are presented for simulation time of 0 and 3.0 ps, respectively.

confined in the vicinity of one H_1 site, TM = Ag, Cr, and Cd; (ii) seven-coordinated isolated single atoms stabilized around the B site via breaking the C-N bonds and serving as TM "glue" to link the neighboring C-N hexagonal rings, TM = Ni, Sc, Ti, V, Fe, Zr, Nb, Rh, Pd, Hf, Ir, and Pt; (iii) dimers nucleated around the B site, with TM = Ru, Mo, Co, Mn, W, and Os; (iv) trimers nucleated around the H_1 site, TM = Au; (v) trimers nucleated around the B site (TM = Cu, Re, Tc, and Ta).

Here we emphasize that, for most of the above TMs that prefer dispersion as single atoms, their positions are confined under the g-C_3N_4 overlayer. First, our calculations demonstrate that, energetically, the TM atoms prefer the interfacial sites around the pores, rather than on the g-C_3N_4 surface; second, it is found that there are negligible diffusion barriers for these studied TM atoms diffuse from the surface site, through the pores of the g-C_3N_4, to the interfacial sites. Therefore, the metal atoms would not coalesce outside the g-C_3N_4/MoS_2 heterojunction. Taking the bond length cutoff of 3.0 Å as a criterion, it is found that in the cases of (i)((ii)), the confined TM single atoms are bonded with one (two) substrate S atoms, six (three) N, and zero (two) C atoms, respectively, as detailed (see Sec. II of the Supplemental Material [73]). Energetically, for most cases, these three confined single TM atoms (TM = Ag, Cr, Cd, Ni, Sc, Ti, V, Fe, Zr, Nb, Rh, Pd, Hf, Ir, and Pt) in (i) and (ii) (see Sec. II of the Supplemental Material, Fig. S3 [73]) are found to be lower in energy by at least 0.5 eV than the formation of dimers or trimers. Moreover, taking TM = Cd as a typical example, we have confirmed that these confined single atoms are prohibited from lateral diffusion between neighboring sites, as manifested by the large (about 2.7 eV) diffusion barrier as shown in Fig. 2(a). In contrast, Cd atoms seem to prefer clustering on pristine MoS_2, as supported by the two following aspects. First, energetically, the nucleation of the two Cd atoms is lower in energy than that of a total separation of the two Cd atoms (Cd-Cd distance is about 10 Å), by about 0.14 eV. Second, kinetically, a Cd atom may smoothly diffuse on pristine 2D MoS_2 and g-C_3N_4 and nucleate, due to the small diffusion barrier (E_{bar}), see Figs. 2(b)–2(c), implying high possibility of clustering as well. Moreover, the thermodynamic stability of Cd_1@g-C_3N_4/MoS_2 complex is further confirmed by *ab initio* molecular dynamic simulations at 500 K [see Fig. 2(d)]. Collectively, these results demonstrate crucial importance of the present heterobilayer in stabilizing the single atoms from clustering.

In the following sections, we focus on the catalytic activities for the cases of 15 TM_1@g-C_3N_4/MoS_2 wherein the TM atoms (TM = Ag, Cr, Cd, Ni, Sc, Ti, V, Fe, Zr, Nb, Rh, Pd, Hf, Ir, and Pt) are stably confined in the interface in formation of single-atom catalytic centers, though single-cluster catalysts [75], such as dimers [76,77] and trimers [78,79] could also exhibit exotic catalysis. Particularly, we examine the possible dynamic behaviors of these confined active centers for O_2 activation and CO oxidation, as proposed in Fig. 1(a). In doing so, based on our extensive calculations, we first systematically screen the adsorptions of O_2 and CO molecules on the confined TM_1 active sites. Note that Ag_1, Ni_1, and Pd_1@g-C_3N_4/MoS_2 are highly inert towards both O_2 activation and CO adsorption with negligible E_{ads} (around 50 meV, not shown here). Moreover, as summarized in Fig. 3, except for Fe, Rh, Ir, and Pt, all other eight TM_1 atoms exhibit larger adsorption energy (E_{ads}) for O_2 than that of CO, which are our main interest of the present study.

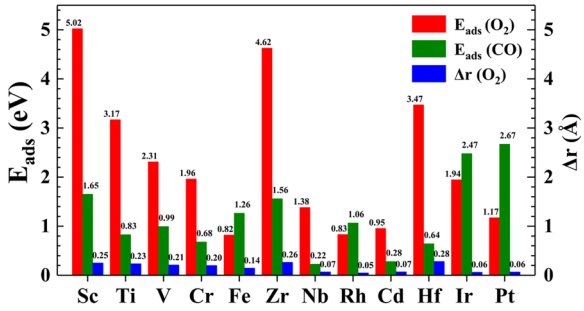

FIG. 3. Adsorption of O_2 and CO on a confined transition metal atom. Calculated adsorption energy (E_{ads}) and O-O bond length enlargement (Δr) for O_2 or CO molecular adsorption on the TM_1@g-C_3N_4/MoS_2 complexes. The bond length changes for CO are not shown, due to their negligible variations.

Now, taking the Nb_1@g-C_3N_4/MoS_2 system consisting of three isolated Nb single atoms confined within the present supercell of heterobilayer (termed Nb_1-SAC) as a typical example, we examine the detailed thermodynamic and kinetic processes of CO oxidation, as schematically shown in Fig. 4. Because CO can hardly coadsorb on the confined Nb_1 reactive site upon the preadsorption of the O_2 molecule due to the significantly low E_{ads} (CO) (see Fig. 3), the Langmuir-Hinshelwood (L-H) process is excluded and only the Eley-Rideal (E-R) mechanism is considered in the following calculations. Taking the optimized Nb_1@g-C_3N_4/MoS_2 as the starting point (i), we find that an incoming O_2 can readily adsorb on the Nb_1 active site, with an E_{ads} of 1.38 eV and enlarged O-O bond length as compared to that in the gas phase, by 0.07 Å [see Fig. 3 and step (ii) in Fig. 4], indicating that the O_2 molecule is significantly activated, which is usually the key step for CO oxidation.

Then, a successively incoming or nearby CO can only very weakly adsorb around the O_2-Nb_1 local structure (see step (iii). However, in further attacking the activated O_2, a low E_{bar} of 0.38 eV is encountered in the transition state (TS_1) with a CO-O_2 distance of 1.86 Å. Afterwards, a CO_2 molecule can be readily released with an exothermic energy of about

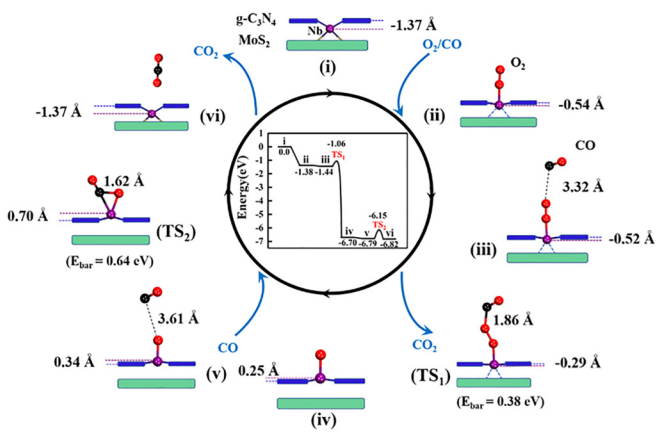

FIG. 4. Schematics of the dynamic behaviors of the Nb_1-SAC confined in the g-C_3N_4/MoS_2 heterobilayer for O_2 activation and CO oxidation via the E-R mechanism.

5.26 eV, leaving a dissociated O atom adsorbed on the Nb_1 active site, see step iv in Fig. 4. Such an atomic O can also be readily attacked by another incoming CO molecule upon overcoming a modest E_{bar} of 0.64 eV in TS_2 with a CO-O distance of 1.62 Å, followed by the release of another CO_2 molecule with an energy gain of about 30 meV, thereby completing the catalytic cycle. Note that in TS_2, the desorption energy of the Nb_1-CO_2 species with the g-C_3N_4/MoS_2 substrate is at least 3.74 eV (see Sec. III of the Supplemental Material, Fig. S4 [73]), demonstrating the stability of the present single atom catalytic centers.

Importantly, the above catalytic cycle for O_2 activation and CO oxidation presented in Fig. 4 vividly confirms the dynamic behaviors of these confined TM_1 active centers as conjectured in Fig. 1(a). Specifically, in structure (i), the Nb_1 single atom (Nb_1-SA) active site is confined about 1.37 Å beneath the mass center of the g-C_3N_4 overlayer, which is selected as the horizon reference, i.e., $\Delta d = -1.37$ Å. Upon O_2 adsorption, the Nb_1-SA is attracted upwards to the g-C_3N_4, by about 0.83 Å. Moreover, in TS_1 for the first round of CO oxidation, the Nb_1-SA further shifts its vertical position to $\Delta d = -0.29$ Å, which is only coordinated with five atoms of the heterobilayer complex. Particularly, in TS_2, the Nb_1-SA active site even migrates outwards to the location above the g-C_3N_4/MoS_2 heterobilayer by about 0.70 Å, becoming fivefold-coordinated with the substrate to facilitate the reaction. Crucially, after completing the CO oxidation cycle, the Nb_1-SA reintegrates back into its stable sandwiched home of the heterobilayer, as schematically presented in step vi of Fig. 4 (and detailed in Sec. IV of the Supplemental Material, Fig. S5 [73]). Similar dynamic processes are also identified for the other TM_1-SAs as established here, such as TM_1@g-C_3N_4/MoS_2 (TM = Cr, Hf, Fe, and Cd), which are representatively detailed for Cr_1@g-C_3N_4/MoS_2(see Sec. IV of the Supplemental Material, Fig. S6 [73]). Therefore, these findings convincingly demonstrate the validity of the proposed concept of DCSAC in enhancing both the stability and catalytic efficiency.

Here, we identify that during the O_2 activation and CO oxidation processes, the single-atom active centers serve as dynamic electronic "antennas" to donate electrons to, or accept electrons from the g-C_3N_4/MoS_2 home as an electron bath, which effectively reduce the reaction barriers. Taking Nb_1-SA again as the prototypical example, our Bader charge analysis shows that each of the three confined Nb atoms donates about 1.7 |e| to the heterobilayer [see Fig. 5(a)], and the g-C_3N_4 overlayer and MoS_2 substrate respectively accommodate about 1.1 and 4.0 |e| from the three deposited Nb atoms. Furthermore, as shown in Fig. 5(b), when O_2 is adsorbed on the Nb_1 reactive site, the O_2 species is extra charged by about 0.676 |e| based on Bader charge analysis; however, the reactive Nb_1 atom only donates about 0.262 |e|, while the other two Nb atoms contribute very minor electron charge. Importantly, the g-C_3N_4 overlayer and MoS_2 substrate contribute 0.177 and 0.265 |e| to the adsorbed O_2, respectively. For CO oxidation, in the TS_1 wherein the Nb_1 atom is shifted out of the interface of the heterobilayer, the g-C_3N_4 overlayer (MoS_2 substrate) donates more electrons, 0.230 (0.398) |e|, to the CO-O_2 complex via the electronic "antenna" of the Nb_1-SA, see Fig. 5(c). In step (iv), the

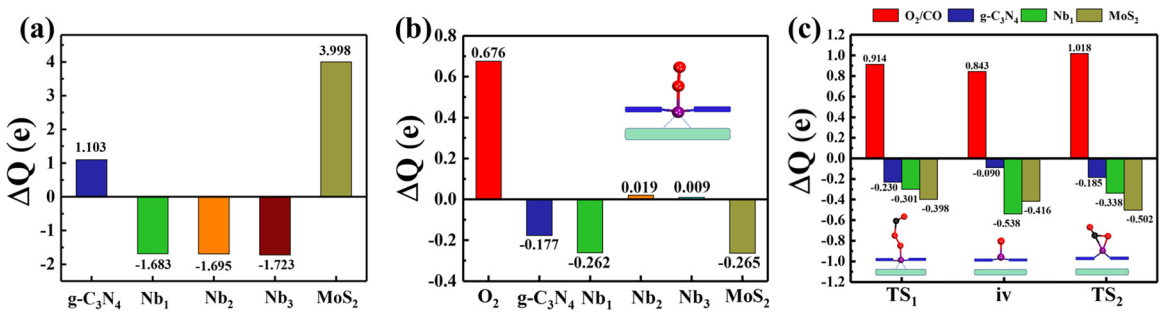

FIG. 5. Dynamic charge transfer for O_2 activation and CO oxidation on Nb_1@g-C_3N_4/MoS_2. Charge transfer analysis for (a) the three deposited Nb single atoms and g-C_3N_4/MoS_2 heterobilayer. (b) O_2 adsorption on the Nb_1 reactive site. (c) the key steps (TS_1, iv, and TS_2) presented in the E-R process of CO oxidation shown in Fig. 4.

g-C_3N_4 donates relatively less electron charge (0.090), whereas Nb_1-SA and the MoS_2 substrate provide significantly more electron charge, 0.538 and 0.416 |e|, respectively; For TS_2, g-C_3N_4 (MoS_2) again contribute 0.185 (0.502) |e|, nevertheless the Nb_1 reactive site donates 0.338 |e|, see Fig. 5(c). That is, the Nb_1-SA reactive site functions as a dynamic electronic "antenna" in donating or accommodating electrons from the adsorbed molecules via tuning its coordination number and the electronic density of state by the Fermi level (see Sec. V of the Supplemental Material, Fig. S7 [73]) by joining force with the g-C_3N_4/MoS_2 heterobilayer. Such an intuitive charge transfer mechanism dominated by the dynamic Nb_1-SA is also observed for other single TM atoms, such as Cr (see Sec. VI of the Supplemental Material, Fig. S8 [73]). Moreover, these results can be conceptually rationalized by recent findings that the catalytic performance of a given active site can be dominated by the dynamic switching of the local coordination environment [34,80,81] and valance state [60,82,83].

We further highlight the importance of the dynamic behaviors of the TM_1-SA reactive sites confined in g-C_3N_4/MoS_2 by comparing the rate-limiting E_{bar} along the optimized minimum energy pathway with that of two other intermediate states with much reduced dynamic shifts of the TM_1 reactive sites, as schematically shown in Figs. 6(a)–6(c). Once again, taking TM = Nb as a typical example, we explore the correlation between the E_{bar} and dynamic shift of the confined TM_1-SA reactive center. In doing so, we consider three representative states: (a) S_0, wherein the reactive Nb_1-SA is constrained in the local structure of the optimized state (OS) of the Nb_1@g-C_3N_4/MoS_2 without any adsorbate, with $\Delta d_{OS} = -1.37$ Å; (b) S_1, wherein Δd is fixed to -0.29 Å; (c) S_2, with the same position as that in the TS_2 shown in Fig. 4, with $\Delta d_{TS} = 0.70$ Å. Clearly, from Fig. 6(d), one can see that the calculated E_{bar} is monotonously reduced from 2.40, through 1.51, to 0.64 eV, when Δd is raised from -1.37, through -0.29, to 0.70 Å, respectively. Therefore, such findings soundly demonstrate the crucial importance of the dynamic behaviors of the TM_1-SA reactive sites in reducing the E_{bar} for CO oxidation.

Close to the end, to further demonstrate the general dynamic features of the TM_1-SA confined in g-C_3N_4/MoS_2, we also examine the calculated Δd in the optimized states (OS) of TM_1@g-C_3N_4/MoS_2 and that in the rate-limiting TS for CO oxidation, with TM = Cr, Nb, Cd, Fe, and Hf. As summarized in Fig. 6(e), in the OS, except for Fe, all other TM_1-SA are confined beneath the mass center of the g-C_3N_4 overlayer. Nevertheless, during the process of CO oxidation, particularly in the TS, the TM_1-SA centers are unexceptionally attracted higher than the mass center of g-C_3N_4. Also for the case of Fe, from OS to TS state, the Δd is also upward shifted from 0.28 to 0.91 Å. More importantly, as shown in Fig. 6(f), we identify that the rate-limiting E_{bar} of these cases are strongly correlated with a descriptor of the relative dynamic shift (RDS) (RDS = $\Delta d_{TS}/(|\Delta d_{OS} - \Delta d_{TS}|)$ of the TM_1-SA, here Δd_{OS} and Δd_{TS} correspond to the position of the TM_1-SA relative to the mass center of the g-C_3N_4 overlayer in the OS and TS states, respectively. It is very clear that, the larger the descriptor of RDS is, the more the electron charge can be transferred from the single-atom catalyst complex to the CO_2 precursor in the transition state (see Sec. VII of the Supplemental Material, Fig. S9 [73]), and the smaller the rate-limiting E_{bar}, demonstrating the general importance of the dynamic confinement of the reactive sites in enhancing the catalytic performance of the SA catalysts. In addition, we have also examined such dynamical behaviors of the present SAC systems by using the RPBE functional [67] (see Sec. VIII of the Supplemental Material, Fig. S10 [73]). The central findings are valid within either computational scheme. Therefore, the present study on the dynamical behaviors of the sandwiched single-atom active sites is characterized by distinctly new and intriguing properties beyond most existing studies of SACs.

To the end, we note that, almost all these DCSAC systems possess net magnetic moments, contributed either by the confined TM single atoms or by the nearby spin-polarized atoms of the g-C_3N_4/MoS_2 heterobilayer (as summarized in Table S1 of Supplemental Material [73]), which ensures that the activation of the spin-triplet ($S = 1$) ground state O_2 molecule to spin-singlet ($S = 0$) excited state proceeds via spin-allowed reaction. Specifically, the Wigner spin selection rule [9,84–89] restricted that the total electron-spin angular momentum of the O_2 molecule and the catalyst system should be conserved in the reaction process. Accordingly, a given catalyst with low spin state (such as $S = 0$) usually exhibit highly inert characteristics toward O_2 activation from $S = 1$ to $S = 0$, otherwise, it would be a spin-forbidden reaction. Therefore, these confined magnetic single-atom catalyst systems also hold great promise in "spin-catalysis" where spin-selection matters [9,89], which are of our great interest in future work.

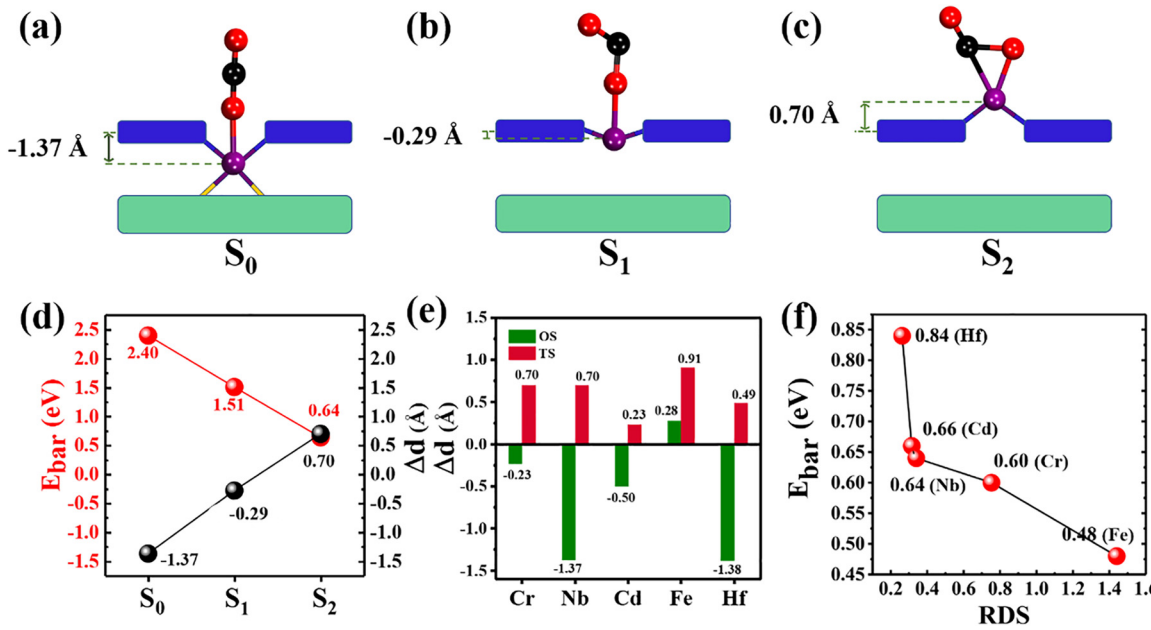

FIG. 6. Illustrations of the dynamic behavior of TM_1-SAC for CO oxidation. Configurations of the rate-limiting steps for CO oxidation with the reactive single atom Nb constrained in (a) with $\Delta d = -1.37$ Å, which is termed the S_0 state, (b) with $\Delta d = -0.29$ Å, S_1, (c) $\Delta d = 0.70$ Å, S_2. (d) Correlation between E_{bar} and Δd for S_0, S_1, and S_2. (e) Δd of the TM atom in the optimized state (OS) of TM_1@g-C_3N_4/MoS_2 and that in the rate-limiting TS of CO oxidation. (f) Correlation between the rate-limiting E_{bar} and relative dynamic shift (RDS) of representative single TM atoms, i.e., $RDS = \Delta d_{TS}/(|\Delta d_{TS} - \Delta d_{OS}|)$.

IV. CONCLUSIONS

In conclusion, using state-of-the-art first-principles calculations, we have proposed a different design principle in stabilizing various low-cost and heavy toxic TMs by dynamically encapsulating such entities within the porous and inherently reactive g-C_3N_4/MoS_2 heterobilayer, and have further demonstrated their ability to act as highly efficient SACs for CO oxidation via a dynamic antenna mechanism. The novelty of the present work on DCSAC lies in: (i) the catalytic single-atom reactive centers are well confined within the interface region of the porous heterobilayer, rather than directly exposed on the surface of the underlying supporting substrates; (ii) the single-atom reactive sites migrate out of the interfacial homes in catalytic reactions, and return to the homes after the reaction is completed; (iii) the single atoms dynamically change their charge states, serving as electronic antennas in donating electrons to or accepting electrons from the reactants, while effectively lowering the reaction barriers. These findings are expected to offer new avenues towards fabrication of highly efficient SAC systems.

ACKNOWLEDGMENTS

We thank Profs. X. G. Gong and C. Shan for helpful discussion. This work was supported by the National Natural Science Foundation of China (Grants No. 12074345, No. 12174349, No. 11804306, and No. 12204421). The calculations were performed on the National Supercomputing Center in Zhengzhou, Henan.

B.J. and F.Z. contributed equally to this work.

[1] B. Qiao, A. Wang, X. Yang, L. F. Allard, Z. Jiang, Y. Cui, J. Liu, J. Li, and T. Zhang, Single-atom catalysis of CO oxidation using Pt_1/FeO_x, Nat. Chem. **3**, 634 (2011).

[2] P. Liu, Y. Zhao, R. Qin, S. Mo, G. Chen, L. Gu, D. M. Chevrier, P. Zhang, Q. Guo, and D. Zang, Photochemical route for synthesizing atomically dispersed palladium catalysts, Science **352**, 797 (2016).

[3] Z. Li, Y. Chen, S. Ji, Y. Tang, W. Chen, A. Li, J. Zhao, Y. Xiong, Y. Wu, Y. Gong, T. Yao, W. Liu, L. Zheng, J. Dong, Y. Wang, Z. Zhuang, W. Xing, C.-T. He, C. Peng, W.-C. Cheong, Q. Li, M. Zhang, Z. Chen, N. Fu, X. Gao, W. Zhu, J. Wan, J. Zhang, L. Gu, S. Wei, P. Hu, J. Luo, J. Li, C. Chen, Q. Peng, X. Duan, Y. Huang, X.-M. Chen, D. Wang, and Y. Li, Iridium single-atom catalyst on nitrogen-doped carbon for formic acid oxidation synthesized using a general host–guest strategy, Nat. Chem. **12**, 764 (2020).

[4] S. K. Kaiser, E. Fako, G. Manzocchi, F. Krumeich, R. Hauert, A. H. Clark, O. V. Safonova, N. López, and J. Pérez-Ramírez, Nanostructuring unlocks high performance of platinum single-atom catalysts for stable vinyl chloride production, Nat. Catal. **3**, 376 (2020).

[5] V. Muravev, G. Spezzati, Y.-Q. Su, A. Parastaev, F.-K. Chiang, A. Longo, C. Escudero, N. Kosinov, and E. J. M. Hensen, Interface dynamics of Pd-CeO_2 single-atom catalysts during CO oxidation, Nat. Catal. **4**, 469 (2021).

[6] Q. Fu and C. Draxl, Hybrid Organic-Inorganic Perovskites as Promising Substrates for Pt Single-Atom Catalysts, Phys. Rev. Lett. **122**, 046101 (2019).

[7] R. A. Bennett, N. D. McCavish, M. Basham, V. R. Dhanak, and M. A. Newton, Structure of Adsorbed Organometallic Rhodium: Model Single Atom Catalysts, Phys. Rev. Lett. **98**, 056102 (2007).

[8] Z. Fu, B. Yang, and R. Wu, Understanding the Activity of Single-Atom Catalysis from Frontier Orbitals, Phys. Rev. Lett. **125**, 156001 (2020).

[9] L. Zhang, X. Ren, X. Zhao, Y. Zhu, R. Pang, P. Cui, Y. Jia, S. Li, and Z. Zhang, Synergetic charge transfer and spin selection in CO oxidation at neighboring magnetic single-atom catalyst sites, Nano Lett. **22**, 3744 (2022).

[10] S. Yang, J. Kim, Y. J. Tak, A. Soon, and H. Lee, Single-atom catalyst of platinum supported on titanium nitride for selective electrochemical reactions, Angew. Chem. Int. Ed. **55**, 2058 (2016).

[11] P. Q. Yin, T. Yao, Y. Wu, L. R. Zheng, Y. Lin, W. Liu, H. X. Ju, J. F. Zhu, X. Hong, Z. X. Deng, G. Zhou, S. Q. Wei, and Y. D. Li, Single cobalt atoms with precise N coordination as superior oxygen reduction reaction catalysts, Angew. Chem. Int. Ed. **55**, 10800 (2016).

[12] Y. J. Chen, S. F. Ji, Y. G. Wang, J. C. Dong, W. X. Chen, Z. Li, R. A. Shen, L. R. Zheng, Z. B. Zhuang, D. S. Wang, and Y. D. Li, Isolated single iron atoms anchored on N-doped porous carbon as an efficient electrocatalyst for the oxygen reduction reaction, Angew. Chem. Int. Ed. **56**, 6937 (2017).

[13] X. Pan and X. Bao, The effects of confinement inside carbon nanotubes on catalysis, Acc. Chem. Res. **44**, 553 (2011).

[14] Q. Fu, F. Yang, and X. Bao, Interface-confined oxide nanostructures for catalytic oxidation reactions, Acc. Chem. Res. **46**, 1692 (2013).

[15] F. Yang, D. Deng, X. Pan, Q. Fu, and X. Bao, Understanding nano effects in catalysis, Natl. Sci. Rev. **2**, 183 (2015).

[16] L. Tang, X. Meng, D. Deng, and X. Bao, Confinement catalysis with 2D materials for energy conversion, Adv. Mater. **31**, 1901996 (2019).

[17] J. Deng, D. Deng, and X. Bao, Robust catalysis on 2D materials encapsulating metals: Concept, application, and perspective, Adv. Mater. **29**, 1606967 (2017).

[18] H. Li, J. Xiao, Q. Fu, and X. Bao, Confined catalysis under two-dimensional materials, Proc. Natl. Acad. Sci. USA **114**, 5930 (2017).

[19] R. T. Mu, Q. Fu, L. Jin, L. Yu, G. Z. Fang, D. L. Tan, and X. H. Bao, Visualizing chemical reactions confined under graphene, Angew. Chem. Int. Ed. **51**, 4856 (2012).

[20] T. Yang, Y. Huang, L. Yang, X. Li, X. Wang, G. Zhang, Y. Luo, and J. Jiang, Protecting single atom catalysts with graphene/carbon-nitride "chainmail", J. Phys. Chem. Lett. **10**, 3129 (2019).

[21] S. Tang, Q. Dang, T. Liu, S. Zhang, Z. Zhou, X. Li, X. Wang, E. Sharman, Y. Luo, and J. Jiang, Realizing a not-strong-not-weak polarization electric field in single-atom catalysts sandwiched by boron nitride and graphene sheets for efficient nitrogen fixation, J. Am. Chem. Soc. **142**, 19308 (2020).

[22] X. Chen, S. Lin, and H. Zhang, Screening of single-atom catalysts sandwiched by boron nitride sheet and graphene for oxygen reduction and oxygen evolution, Renew. Energ. **189**, 502 (2022).

[23] J. M. Thomas, R. Raja, and D. W. Lewis, Single-site heterogeneous catalysts, Angew. Chem. Int. Ed. **44**, 6456 (2005).

[24] J. M. Thomas, Z. Saghi, and P. L. Gai, Can a single atom serve as the active site in some heterogeneous catalysts? Top. Catal. **54**, 588 (2011).

[25] X.-F. Yang, A. Wang, B. Qiao, J. Li, J. Liu, and T. Zhang, Single-atom catalysts: A new frontier in heterogeneous catalysis, Acc. Chem. Res. **46**, 1740 (2013).

[26] C. Copéret, Single-sites and nanoparticles at tailored interfaces prepared via surface organometallic chemistry from thermolytic molecular precursors, Acc. Chem. Res. **52**, 1697 (2019).

[27] C. Copéret, A. Comas-Vives, M. P. Conley, D. P. Estes, A. Fedorov, V. Mougel, H. Nagae, F. Núñez-Zarur, and P. A. Zhizhko, Surface organometallic and coordination chemistry toward single-site heterogeneous catalysts: Strategies, methods, structures, and activities, Chem. Rev. **116**, 323 (2016).

[28] W. E. Kaden, T. Wu, W. A. Kunkel, and S. L. Anderson, Electronic structure controls reactivity of size-selected Pd clusters adsorbed on TiO_2 surfaces, Science **326**, 826 (2009).

[29] A. A. Herzing, C. J. Kiely, A. F. Carley, P. Landon, and G. J. Hutchings, Identification of active gold nanoclusters on iron oxide supports for CO oxidation, Science **321**, 1331 (2008).

[30] S. F. Li, X. J. Zhao, X. S. Xu, Y. F. Gao, and Z. Zhang, Stacking Principle and Magic Sizes of Transition Metal Nanoclusters Based on Generalized Wulff Construction, Phys. Rev. Lett. **111**, 115501 (2013).

[31] S. B. Vendelbo, C. F. Elkjær, H. Falsig, I. Puspitasari, P. Dona, L. Mele, B. Morana, B. J. Nelissen, R. van Rijn, J. F. Creemer, P. J. Kooyman, and S. Helveg, Visualization of oscillatory behaviour of Pt nanoparticles catalysing CO oxidation, Nat. Mater. **13**, 884 (2014).

[32] C. T. Campbell, S. C. Parker, and D. E. Starr, The effect of size-dependent nanoparticle energetics on catalyst sintering, Science **298**, 811 (2002).

[33] S. Cao, Y. Zhao, S. Lee, S. Yang, J. Liu, G. Giannakakis, M. Li, M. Ouyang, D. Wang, and E. C. H. Sykes, High-loading single Pt atom sites [Pt-$O(OH)_x$] catalyze the CO PROX reaction with high activity and selectivity at mild conditions, Sci. Adv. **6**, eaba3809 (2020).

[34] R. Qin, K. Liu, Q. Wu, and N. Zheng, Surface coordination chemistry of atomically dispersed metal catalysts, Chem. Rev. **120**, 11810 (2020).

[35] C. Copéret, W.-C. Liao, C. P. Gordon, and T.-C. Ong, Active sites in supported single-site catalysts: An NMR perspective, J. Am. Chem. Soc. **139**, 10588 (2017).

[36] W. Gao, S. Li, H. He, X. Li, Z. Cheng, Y. Yang, J. Wang, Q. Shen, X. Wang, Y. Xiong, Y. Zhou, and Z. Zou, Vacancy-defect modulated pathway of photoreduction of CO_2 on single atomically thin $AgInP_2S_6$ sheets into olefiant gas, Nat. Commun. **12**, 4747 (2021).

[37] T. Kosmala, A. Baby, M. Lunardon, D. Perilli, H. Liu, C. Durante, C. Di Valentin, S. Agnoli, and G. Granozzi, Operando visualization of the hydrogen evolution reaction with atomic-scale precision at different metal–graphene interfaces, Nat. Catal. **4**, 850 (2021).

[38] F. Dvořák, M. F. Camellone, A. Tovt, N.-D. Tran, F. R. Negreiros, M. Vorokhta, T. Skála, I. Matolínová, J. Mysliveček,

and V. Matolín, Creating single-atom Pt-ceria catalysts by surface step decoration, Nat. Commun. **7**, 10801 (2016).

[39] D. Kunwar, S. Zhou, A. DeLaRiva, E. J. Peterson, H. Xiong, X. I. Pereira-Hernández, S. C. Purdy, R. ter Veen, H. H. Brongersma, J. T. Miller, H. Hashiguchi, L. Kovarik, S. Lin, H. Guo, Y. Wang, and A. K. Datye, Stabilizing high hetal loadings of thermally stable platinum single atoms on an industrial catalyst support, ACS Catal. **9**, 3978 (2019).

[40] R. T. Hannagan, G. Giannakakis, R. Réocreux, J. Schumann, J. Finzel, Y. Wang, A. Michaelides, P. Deshlahra, P. Christopher, and M. Flytzani-Stephanopoulos, First-principles design of a single-atom–alloy propane dehydrogenation catalyst, Science **372**, 1444 (2021).

[41] M. D. Marcinkowski, M. T. Darby, J. Liu, J. M. Wimble, F. R. Lucci, S. Lee, A. Michaelides, M. Flytzani-Stephanopoulos, M. Stamatakis, and E. C. H. Sykes, Pt/Cu single-atom alloys as coke-resistant catalysts for efficient C–H activation, Nat. Chem. **10**, 325 (2018).

[42] S. J. Tauster, S. C. Fung, and R. L. Garten, Strong metal-support interactions. Group 8 noble metals supported on titanium dioxide, J. Am. Chem. Soc. **100**, 170 (1978).

[43] A. Bruix, J. A. Rodriguez, P. J. Ramirez, S. D. Senanayake, J. Evans, J. B. Park, D. Stacchiola, P. Liu, J. Hrbek, and F. Illas, A new type of strong metal-support interaction and the production of H_2 through the transformation of water on $Pt/CeO_2(111)$ and $Pt/CeO_x/TiO_2(110)$ catalysts, J. Am. Chem. Soc. **134**, 8968 (2012).

[44] C. T. Campbell, Catalyst-support interactions: Electronic perturbations, Nat. Chem. **4**, 597 (2012).

[45] J. Gu, M. Jian, L. Huang, Z. Sun, A. Li, Y. Pan, J. Yang, W. Wen, W. Zhou, Y. Lin, H.-J. Wang, X. Liu, L. Wang, X. Shi, X. Huang, L. Cao, S. Chen, X. Zheng, H. Pan, J. Zhu, S. Wei, W.-X. Li, and J. Lu, Synergizing metal–support interactions and spatial confinement boosts dynamics of atomic nickel for hydrogenations, Nat. Nanotechnol. **16**, 1141 (2021).

[46] C. Zhu, S. Fu, Q. Shi, D. Du, and Y. Lin, Single-atom electrocatalysts, Angew. Chem. Int. Ed. **56**, 13944 (2017).

[47] J. Zhao and Z. Chen, Single Mo atom supported on defective boron nitride monolayer as an efficient electrocatalyst for nitrogen fixation: A computational study, J. Am. Chem. Soc. **139**, 12480 (2017).

[48] C. Choi, G. H. Gu, J. Noh, H. S. Park, and Y. Jung, Understanding potential-dependent competition between electrocatalytic dinitrogen and proton reduction reactions, Nat. Commun. **12**, 4353 (2021).

[49] C. Xia, Y. Qiu, Y. Xia, P. Zhu, G. King, X. Zhang, Z. Wu, J. Y. Kim, D. A. Cullen, D. Zheng, P. Li, M. Shakouri, E. Heredia, P. Cui, H. N. Alshareef, Y. Hu, and H. Wang, General synthesis of single-atom catalysts with high metal loading using graphene quantum dots, Nat. Chem. **13**, 887 (2021).

[50] C. Zhao, X. Dai, T. Yao, W. Chen, X. Wang, J. Wang, J. Yang, S. Wei, Y. Wu, and Y. Li, Ionic exchange of metal–organic frameworks to access single nickel sites for efficient electroreduction of CO_2, J. Am. Chem. Soc. **139**, 8078 (2017).

[51] Q. He, D. B. Liu, J. H. Lee, Y. M. Liu, Z. H. Xie, S. Hwang, S. Kattel, L. Song, and J. G. G. Chen, Electrochemical conversion of CO_2 to syngas with controllable CO/H_2 ratios over Co and Ni single-atom catalysts, Angew. Chem. Int. Ed. **59**, 3033 (2020).

[52] S. Mitchell and J. Pérez-Ramírez, Single atom catalysis: A decade of stunning progress and the promise for a bright future, Nat. Commun. **11**, 4302 (2020).

[53] D. Deng, L. Yu, X. Chen, G. Wang, L. Jin, X. Pan, J. Deng, G. Sun, and X. Bao, Iron encapsulated within pod-like carbon nanotubes for oxygen reduction reaction, Angew. Chem. Int. Ed. **52**, 371 (2013).

[54] Q. Fu and X. Bao, Surface chemistry and catalysis confined under two-dimensional materials, Chem. Soc. Rev. **46**, 1842 (2017).

[55] Y. Wang, J. Mao, X. Meng, L. Yu, D. Deng, and X. Bao, Catalysis with two-dimensional materials confining single atoms: Concept, design, and applications, Chem. Rev. **119**, 1806 (2019).

[56] A. Alarawi, V. Ramalingam, and J.-H. He, Recent advances in emerging single atom confined two-dimensional materials for water splitting applications, Mater. Today Energy **11**, 1 (2019).

[57] D. Deng, X. Chen, L. Yu, X. Wu, Q. Liu, Y. Liu, H. Yang, H. Tian, Y. Hu, P. Du, R. Si, J. Wang, X. Cui, H. Li, J. Xiao, T. Xu, J. Deng, F. Yang, N. Duchesne Paul, P. Zhang, J. Zhou, L. Sun, J. Li, X. Pan, and X. Bao, A single iron site confined in a graphene matrix for the catalytic oxidation of benzene at room temperature, Sci. Adv. **1**, e1500462 (2015).

[58] P. Peng, L. Shi, F. Huo, C. Mi, X. Wu, S. Zhang, and Z. Xiang, A pyrolysis-free path toward superiorly catalytic nitrogen-coordinated single atom, Sci. Adv. **5**, eaaw2322 (2019).

[59] C.-X. Zhao, J.-N. Liu, J. Wang, C. Wang, X. Guo, X.-Y. Li, X. Chen, L. Song, B.-Q. Li, and Q. Zhang, A clicking confinement strategy to fabricate transition metal single-atom sites for bifunctional oxygen electrocatalysis, Sci. Adv. **8**, eabn5091 (2022).

[60] H. Peng, I. G. McKendry, R. Ding, A. C. Thenuwara, Q. Kang, S. L. Shumlas, D. R. Strongin, M. J. Zdilla, and J. P. Perdew, Redox properties of birnessite from a defect perspective, Proc. Natl. Acad. Sci. USA **114**, 9523 (2017).

[61] Y. G. Wang, D. H. Mei, V. A. Glezakou, J. Li, and R. Rousseau, Dynamic formation of single-atom catalytic active sites on ceria-supported gold nanoparticles, Nat. Commun. **6**, 6511 (2015).

[62] W. Fu, H. He, Z. Zhang, C. Wu, X. Wang, H. Wang, Q. Zeng, L. Sun, X. Wang, J. Zhou, Q. Fu, P. Yu, Z. Shen, C. Jin, B. I. Yakobson, and Z. Liu, Strong interfacial coupling of MoS_2/g-C_3N_4 van de Waals solids for highly active water reduction, Nano Energy **27**, 44 (2016).

[63] P. Hohenberg and W. Kohn, Inhomogeneous electron gas, Phys. Rev. **136**, B864 (1964).

[64] G. Kresse and J. Furthmüller, Efficient iterative schemes for *ab initio* total-energy calculations using a plane-wave basis set, Phys. Rev. B **54**, 11169 (1996).

[65] P. E. Blöchl, Projector augmented-wave method, Phys. Rev. B **50**, 17953 (1994).

[66] J. P. Perdew, K. Burke, and M. Ernzerhof, Generalized Gradient Approximation Made Simple, Phys. Rev. Lett. **77**, 3865 (1996).

[67] B. Hammer, L. B. Hansen, and J. K. Nørskov, Improved adsorption energetics within density-functional theory using revised Perdew-Burke-Ernzerhof functionals, Phys. Rev. B **59**, 7413 (1999).

[68] X. Wang, K. Maeda, A. Thomas, K. Takanabe, G. Xin, J. M. Carlsson, K. Domen, and M. Antonietti, A metal-free polymeric

photocatalyst for hydrogen production from water under visible light, Nat. Mater. **8**, 76 (2009).

[69] S. Grimme, J. Antony, S. Ehrlich, and H. Krieg, A consistent and accurate *ab initio* parametrization of density functional dispersion correction (DFT-D) for the 94 elements H-Pu, J. Chem. Phy. **132**, 154104 (2010).

[70] S. Grimme, S. Ehrlich, and L. Goerigk, Effect of the Damping Function in Dispersion Corrected Density Functional Theory, J. Comput. Chem. **32**, 1456 (2011).

[71] G. Henkelman and H. Jonsson, Improved tangent estimate in the nudged elastic band method for finding minimum energy paths and saddle points, J. Chem. Phys. **113**, 9978 (2000).

[72] G. Henkelman, B. P. Uberuaga, and H. Jónsson, A climbing image nudged elastic band method for finding saddle points and minimum energy paths, J. Chem. Phys. **113**, 9901 (2000).

[73] See Supplemental Material at http://link.aps.org/supplemental/10.1103/PhysRevB.107.205421 for the optimized geometric structures of g-C_3N_4/MoS_2 and TM-C_3N_4/MoS_2 complexes, the coordinates of representative TM_1-C_3N_4/MoS_2 complexes, electronic structure analysis, etc.

[74] L. Zhang, P. Bampoulis, A. N. Rudenko, Q. Yao, A. van Houselt, B. Poelsema, M. I. Katsnelson, and H. J. W. Zandvliet, Structural and Electronic Properties of Germanene on MoS_2, Phys. Rev. Lett. **116**, 256804 (2016).

[75] S. Zhang, L. Nguyen, J.-X. Liang, J. Shan, J. Liu, A. I. Frenkel, A. Patlolla, W. Huang, J. Li, and F. Tao, Catalysis on singly dispersed bimetallic sites, Nat. Commun. **6**, 7938 (2015).

[76] Y. Wang, L. Cao, N. J. Libretto, X. Li, C. Li, Y. Wan, C. He, J. Lee, J. Gregg, H. Zong, D. Su, J. T. Miller, T. Mueller, and C. Wang, Ensemble effect in bimetallic electrocatalysts for CO_2 reduction, J. Am. Chem. Soc. **141**, 16635 (2019).

[77] L. Zhang, R. Si, H. Liu, N. Chen, Q. Wang, K. Adair, Z. Wang, J. Chen, Z. Song, J. Li, M. N. Banis, R. Li, T.-K. Sham, M. Gu, L.-M. Liu, G. A. Botton, and X. Sun, Atomic layer deposited Pt-Ru dual-metal dimers and identifying their active sites for hydrogen evolution reaction, Nat. Commun. **10**, 4936 (2019).

[78] S. Dai, J.-P. Chou, K.-W. Wang, Y.-Y. Hsu, A. Hu, X. Pan, and T.-Y. Chen, Platinum-trimer decorated cobalt-palladium core-shell nanocatalyst with promising performance for oxygen reduction reaction, Nat. Commun. **10**, 440 (2019).

[79] P. Liu, X. Huang, D. Mance, and C. Copéret, Atomically dispersed iridium on MgO(111) nanosheets catalyses benzene–ethylene coupling towards styrene, Nat. Catal. **4**, 968 (2021).

[80] H. Xu, D. Cheng, D. Cao, and X. C. Zeng, A universal principle for a rational design of single-atom electrocatalysts, Nat. Catal. **1**, 339 (2018).

[81] X. Li, L. Liu, X. Ren, J. Gao, Y. Huang, and B. Liu, Microenvironment modulation of single-atom catalysts and their roles in electrochemical energy conversion, Sci. Adv. **6**, eabb6833 (2020).

[82] G. Wu, X. Zheng, P. Cui, H. Jiang, X. Wang, Y. Qu, W. Chen, Y. Lin, H. Li, X. Han, Y. Hu, P. Liu, Q. Zhang, J. Ge, Y. Yao, R. Sun, Y. Wu, L. Gu, X. Hong, and Y. Li, A general synthesis approach for amorphous noble metal nanosheets, Nat. Commun. **10**, 4855 (2019).

[83] J. Wang, Z. Jiang, G. Peng, E. Hoenig, G. Yan, M. Wang, Y. Liu, X. Du, and C. Liu, Surface valence state effect of MoO^{2+x} on electrochemical nitrogen reduction, Adv. Sci. **9**, 2104857 (2022).

[84] E. Wigner and E. E. Witmer, Uber die Struktur der zweiatomigen Molekelspektren nach der Quantenmechanik, Z. Phys. **51**, 859 (1928).

[85] J. H. Moore, Jr., Investigation of the Wigner spin rule in collisions of N^+ with He, Ne, Ar, N_2, and O_2, Phys. Rev. A **8**, 2359 (1973).

[86] J. Behler, B. Delley, S. Lorenz, K. Reuter, and M. Scheffler, Dissociation of O_2 at Al(111): The Role of Spin Selection Rules, Phys. Rev. Lett. **94**, 036104 (2005).

[87] R. Burgert, H. Schnockel, A. Grubisic, X. Li, S. T. Stokes, K. H. Bowen, G. F. Gantefor, B. Kiran, and P. Jena, Spin conservation accounts for aluminum cluster anion reactivity pattern with O_2, Science **319**, 438 (2008).

[88] C. Carbogno, J. Behler, A. Gross, and K. Reuter, Fingerprints for Spin-Selection Rules in the Interaction Dynamics of O_2 at Al(111), Phys. Rev. Lett. **101**, 096104 (2008).

[89] Y. Y. Wang, X. Y. Ren, B. J. Jiang, M. Deng, X. J. Zhao, R. Pang, and S. Li, Synergetic catalysis of magnetic single-atom catalysts confined in graphitic-C_3N_4/CeO_2(111) heterojunction for CO oxidization, J. Phys. Chem. Lett. **13**, 6367 (2022).